Quantifying Event-Based Heatwave-Induced Power Outage Risk: A Multi-Year Spatiotemporal Analysis in Texas

S. M. Redwan Kabir , Mizanur Rahman * , Farhana Kabir Zisha , Lei Meng

Posted Date: 8 April 2026

doi: 10.20944/preprints202604.0453.v1

Keywords: heatwave; power outage; Texas; EAGLE-I; heat index; logistic regression; spatiotemporal analysis; climate resilience; electric distribution; outage risk

 doi:10.20944/preprints202604.0453.v1

Article

Quantifying Event-Based Heatwave-Induced Power Outage Risk: A Multi-Year Spatiotemporal Analysis in Texas

S. M. Redwan Kabir [1], Mizanur Rahman [1,*], Farhana Kabir Zisha [1] and Lei Meng [1]

[1] School of Environment, Geography, and Sustainability, Western Michigan University, Kalamazoo, MI 49008, USA

* Correspondence: mizanur.rahman@wmich.edu

Abstract

Heatwaves are intensifying across the southern United States, particularly in Texas, placing unprecedented stress on electric distribution networks and increasing power outage risk. Yet the relationship between heatwave characteristics and observed outages remains poorly quantified at multi-year, statewide scales. This study develops an event-based, spatiotemporal framework to quantify heatwave-induced outage risk across 254 Texas counties from 2014–2021 by integrating county-level EAGLE-I outage records with reanalysis-derived heat index measurements. An adaptive percentile-based threshold identifies heatwave days and constructs multi-day events, from which event-level metrics duration, mean heat index, and maximum customers affected are derived. Across 3,048 identified heatwave events, 51% involved at least one outage, revealing widespread heat-related reliability challenges. Spatial indicators show substantial heterogeneity: some counties experience frequent minor outages, while major population exposure is concentrated in large urban load centers. Outage severity and duration exhibit heavy-tailed distributions, with a small number of extreme events disproportionately affecting customers. Logistic regression models under three severity definitions (P90, P95, and ≥500 customers) demonstrate that heat intensity is a significant probabilistic driver of major outages, with each +1 °F increase in mean event heat index raising the odds by approximately 43–52%. These findings offer a scalable methodology for climate-related reliability assessment, supporting grid hardening, resource planning, and public-health preparedness.

Keywords: heatwave; power outage; Texas; EAGLE-I; heat index; logistic regression; spatiotemporal analysis; climate resilience; electric distribution; outage risk

1. Introduction

Extreme heatwaves have emerged as one of the most consequential climate-related hazards of the twenty-first century, with far-reaching impacts on public health, ecosystems, economic productivity, and the reliability of critical infrastructure systems [1]. Driven by anthropogenic climate change, the frequency, intensity, and persistence of heatwaves have increased markedly across the United States and globally, a trend expected to accelerate in coming decades [2,3]. This escalation raises urgent concerns for communities, policymakers, and utility operators seeking to safeguard public welfare and sustain economic activity under extreme thermal stress. Reliable electricity is foundational to modern society, supporting essential services such as cooling, healthcare, communications, and transportation. As heatwaves intensify, the resilience of electric power distribution networks becomes a central public safety and infrastructure-planning concern.

Heatwaves impose significant physiological stress on human populations and negatively affect ecosystems. At the biological level, heat exposure increases dehydration, blood viscosity, and platelet activation, elevating risks of ischemic stroke and cardiovascular events [4]. Urban populations face

 doi:10.20944/preprints202604.0453.v1

disproportionately severe impacts due to the urban heat island effect, which exacerbates indoor and outdoor temperature exposures and contributes to elevated morbidity and mortality [4]. Ecosystems are similarly vulnerable: marine heatwaves are projected to accelerate the loss of Mediterranean seagrass meadows, threatening fisheries, coastal protection, and ecosystem stability [3,5]. On land, vegetation stress reduces evapotranspiration cooling, weakening nature-based heat mitigation benefits and diminishing the ecological resilience of green infrastructure [6].

Heatwaves also increasingly disrupt electricity systems, which experience simultaneous surges in cooling demand and reductions in supply capacity. High temperatures dramatically elevate residential and commercial cooling loads [7]. At the same time, thermal and hydropower plants struggle to maintain output due to reduced cooling efficiency and declining water availability, while transmission lines experience reduced ampacity [7–9]. These conditions heighten grid vulnerability, elevate the probability of operational failures, and increase the likelihood of cascading outages. Satellite evidence further shows abrupt spikes in SO_2 and NO_2 emissions from power plants during heatwaves, driven by amplified fossil-fuel generation to meet escalating demand an overlooked feedback loop that worsens air quality and deepens grid stress [10].

Empirical studies confirm that heatwaves directly increase both the frequency and duration of power outages. In China, heatwaves were found to increase outages by up to 4%, with an additional heatwave day raising outage probability by 0.5% [11]. Similar trends are observed in the United States, where county-level power system vulnerability has steadily increased, especially in regions with high climatic exposure and socio-demographic vulnerabilities [12]. Urban and low-income communities are disproportionately impacted, experiencing higher outage-related risk and reduced adaptive capacity [13]. The human consequences of such failures are severe: simulated concurrent heatwave–blackout scenarios more than doubled mortality and caused up to 50% of Phoenix residents to require medical care [14]. Heatwave-driven health burdens can also escalate rapidly, underpinning the need for robust prediction and early-warning systems[15].

Moreover, heatwaves rarely occur in isolation. They frequently interact with droughts, high winds, heavy precipitation, and other hazards to produce compound events with severe socio-economic consequences [16]. The 2022 drought–heatwave crisis exemplified these dynamics: simultaneous hydropower shortages and heat-driven demand surges led to an 11-day industrial shutdown and more than 66 billion CNY in indirect economic losses in Sichuan province of China [3]. Marine heatwaves have also been linked to rapid intensification of tropical cyclones, further compounding vulnerability to infrastructure collapse [17]. On longer timescales, heatwaves impose substantial economic burdens; climate-extreme assessments in Hainan of China revealed escalating losses from heatwaves, droughts, and extreme rainfall [18]. Systematic reviews emphasize that these burdens fall disproportionately on socioeconomically disadvantaged populations [3].

Despite these advances, a critical research gap persists: the relationship between heatwave characteristics such as intensity, duration, and spatial extent and observed power outage behavior remains poorly quantified. Most prior research on grid resilience has focused on acute storm events, employing event-based or probabilistic frameworks to model outage likelihood, spatial distribution, and restoration timelines [19,20]. Parallel heatwave research has emphasized human health, thermal indices, predicting or climate trends which often overlook the cumulative and prolonged impacts of extreme heat on aging electric distribution systems [21,22]. Many analyses also rely on fixed temperature thresholds or calendar-based definitions of heatwaves, which inadequately capture regional climatic variability. Furthermore, existing studies rarely integrate adaptive heatwave definitions with high-resolution outage data, leaving substantial gaps in understanding the spatiotemporal dynamics of heat-driven grid failures.

This gap is particularly significant in Texas, characterized by diverse climatic zones, rapidly growing electricity demand, decentralized grid architecture, and recurrent exposure to extreme heat [23]. The operational complexity of Texas's electric distribution systems, combined with its large spatial extent and socio-demographic diversity, makes it an ideal setting for investigating heatwave–outage interactions.

 doi:10.20944/preprints202604.0453.v1

To address these deficiencies, the present study develops a multi-year, event-based spatiotemporal framework integrating county-level outage data from the EAGLE-I system with reanalysis-grade meteorological datasets. Adaptive, percentile-based heatwave thresholds are applied to construct multi-day events that capture locally relevant variability in heat intensity and duration. We linked these events to outage metrics including frequency, severity, population exposure, and restoration duration allowing examination of how heat-driven risks manifest across space and time. We employed Logistic regression models to estimate the probability that heatwaves escalate into major outages, under multiple severity definitions, capturing nonlinear relationships between thermal stress and infrastructure failure.

This research leverages a multi-year, statewide dataset of high-resolution outage and open-source climate records to evaluate risk through an adaptive heatwave detection approach within a probabilistic risk framework. By distinguishing between heatwave attributes and linking them directly to observed outage behavior, this research provides a robust, scalable methodology for evaluating climate-induced grid vulnerabilities. Key contributions include: (i) a comprehensive, event-based characterization of heatwave-induced outages across Texas; (ii) introduction of an adaptive heatwave-detection method tailored to regional climatology and grid-reliability concerns; (iii) probabilistic evidence demonstrating that heat intensity is a significant predictor of major outages; and (iv)reproducible modeling tools for assessing climate-related risks in electric power systems. These contributions advance scientific understanding of heatwave-driven outage dynamics and support future planning for climate-resilient energy infrastructure, emergency response strategies, and public-health preparedness.

The remainder of this paper is organized as follows: Section 2 describes the data sources and analytical methods used to construct the event-based framework. Section 3 presents the results, including spatial patterns of outage risk and the probabilistic relationship between heat intensity and major outages. Section 4 discusses the implications for grid resilience, policy, and future research. Section 5 concludes with recommendations for infrastructure planning and climate adaptation.

2. Materials and Methods

2.1. Study Area and Period

This study focuses on the risk of heatwave-induced power outage in all counties within Texas, USA, over 2014–2021. Texas is highly exposed to extreme heat and has a large, spatially diverse distribution network, making it an informative test bed for compound heat–infrastructure risk. All computations were performed at the county level (254 counties), using 2018 U.S. Census Bureau cartographic boundary shapefiles for geometries in Figure 1.

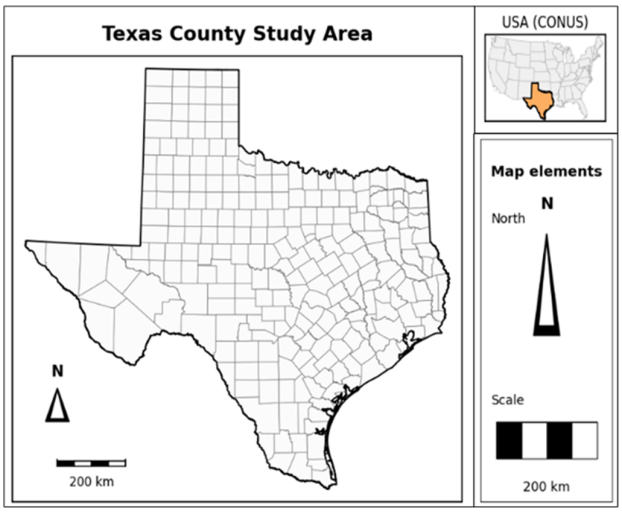

 doi:10.20944/preprints202604.0453.v1

Figure 1. *Study Area Map; Data: U.S. Census Bureau TIGER/Line, generalized county & state boundaries; Projection: NAD83 / Texas Centric Albers Equal Area (EPSG:3083).*

We examined heat and outage conditions at an event scale primarily driven by multi-day heatwaves and then aggregated to the county level to construct spatial indicators of heat-related outage risk. The temporal resolution is hourly for raw meteorology and outage records, and daily for derived metrics and heatwave events. The warm season is defined as May–September, consistent with heat-health and heatwave climatology for the U.S. [2,24].

2.2. Electricity Outage Data and Event Construction

2.2.1. EAGLE-I Data and Hourly Aggregation

We used distribution-level outage records from the EAGLE-I (Environment for Analysis of Geo-Located Energy Information) system [25,26], which aggregates outage information scraped from utilities' public outage maps via an ETL process and reports, for each timestamp, the number of customers without power in each U.S. county perFIPS code. For each year y ∈ [2014,2021], we obtained a CSV file containing county FIPS code, county name, state code, a timestamp t (run_start_time), and and the corresponding count of affected customers (sum) in county c. The eight-year study window (2014–2021) was chosen because it represents the full extent of publicly released EAGLE-I data at the time of analysis [25], providing sufficient temporal depth to capture inter-annual variability in both heatwave occurrence and outage patterns. Records were filtered to retain only Texas counties (state label "Texas" or "TX"), and all timestamps were parsed into datetime format. Texas was chosen as the study domain because it operates a largely self-contained electricity grid (ERCOT) that has experienced multiple high-profile heatwave-related reliability events [11,23,26], making it an ideal setting for examining heat–outage relationships without the confounding effects of inter-regional power transfers. Because the EAGLE-I system reports at irregular sub-hourly intervals (approximately every 10–15 min), raw records cannot be directly merged with standard hourly meteorological data. We therefore aggregated to county–hour peaks:$outage\_customers_{c,h} = \max_{t \in h}(sum_{c,t})$; where c denotes a county and h indexes each hour. The operator $\max_{t \in h}$ selects the largest reported customer count across all timestamps t falling within hour h, thereby capturing the worst-case concurrent outage exposure within that hour. The maximum (rather than the mean or sum) was chosen because it reflects the peak instantaneous stress on distribution infrastructure, the quantity most relevant to system operators assessing grid reliability during extreme weather [19,20]. This peak-based hourly aggregation also aligns outage data with the hourly temporal resolution of the meteorological inputs (Section 2.3), ensuring consistent temporal granularity across all datasets.

2.2.2. New Outages

To distinguish new outage occurrences from ongoing or restored outages, we derived hourly new outages as the positive first difference of the customer outage count within each county: [

$$new\_customers_{c,h} = \max(0,\ \text{outages\_customers}_{c,h} - \text{outages\_customer}_{c,h-1})$$

Negative differences (power restoration) are clipped to zero to avoid counting the same outage twice. Hours without any EAGLE-I record for a county are treated as zero outages (i.e., $outage\_customers_{c,h}$ = 0). This first-differencing approach was adopted because the raw EAGLE-I data report cumulative (stock) counts of customers without power at each snapshot, conflating new failures with ongoing outages and restorations [27]. By extracting only positive increments, the derived variable isolates the timing and magnitude of new failure events information that is essential for establishing temporal links between weather triggers and infrastructure failures. This event-onset representation is consistent with prior power-system resilience studies that model

 doi:10.20944/preprints202604.0453.v1

outage occurrence and severity at the event level and it avoids the well-known problem of attributing restorations to weather conditions that occur hours or days after the initiating event. [16,19].

2.3. Meteorological Data and Apparent Temperature

2.3.1. Open-Meteo Archive

We obtained weather data from the Open-Meteo archive API, which provides hourly air temperature T (°C) and relative humidity RH (%) from ERA5 global reanalysis (ECMWF Reanalysis v5). ERA5 was selected as the weather data source because it provides globally consistent, quality-controlled, hourly atmospheric variables at 0.25° spatial resolution from 1940 to the near-present, and it has been extensively validated for temperature and humidity over the continental United States [28]. A central point in Texas (31°N, 99°W) was selected to represent statewide weather from 2014–2021 while all data were requested in the UTC time zone. While Texas spans multiple climate zones with spatial gradients in temperature and humidity, heatwave episodes at the statewide scale are predominantly driven by synoptic-scale high-pressure systems that produce broadly coherent warming across the state rather than purely local forcing. This approach is consistent with Texas heatwave analyses that treat major heat events as synoptic-scale phenomena affecting the state coherently, despite local spatial heterogeneity [26]. A single central point therefore captures the large-scale thermal forcing that drives regional heatwave days, even though it cannot resolve intra-state spatial heterogeneity.

The use of a regional average rather than a single point was considered; however, his design choice also ensures that any observed relationship between heat intensity and outage probability reflects the large-scale thermal forcing common to all counties, rather than being confounded by spatially varying weather inputs. We acknowledge this simplification as a limitation in Section 4.4. We applied the hourly data uniformly to all counties. This approach does not account for fine-scale spatial variability but captures the large-scale heat patterns responsible for regional heatwaves, consistent with risk-assessment methods linking gridded weather data with infrastructure outcomes [16,21,29,30].

To validate this approach, we conducted spatial coherence analysis across eight representative locations spanning Texas's diverse climate zones: humid subtropical (Houston/Gulf Coast, Dallas/North Texas, Corpus Christi/Coastal), semi-arid (San Antonio/South-Central, Amarillo/Panhandle, Midland/West Texas), arid (El Paso/Far West), and central plains (reference point). For each location, we extracted hourly temperature and relative humidity from ERA5 via Open-Meteo and computed daily maximum heat index values for the study period. Detailed results are described in Section 3.1.

2.3.2. Dew Point and Heat Index

Dew-point temperature T_d was computed from the hourly temperature and relative humidity at the central reference point (31.0°N, 99.0°W) using the Magnus-Tetens approximation [31]:

$$\gamma\,(T, RH) = \frac{\alpha T}{b+T} + ln\left(\frac{RH}{100}\right)$$

$$T_d = \frac{\beta\gamma}{\alpha-\gamma}$$ where α=17.27, β=237.7 °C, T is air temperature in °C, and RH is relative humidity in percent. The Magnus–Tetens formula was chosen because it provides an accurate closed-form approximation of the Clausius–Clapeyron relation for the range of temperatures encountered in Texas summers, with errors below 0.4 °C for temperatures between −45 °C and 60 °C [31]. The dew point was then converted to Fahrenheit ($T_{d,f} = T_d$ x 9/5 + 32) and replicated to all counties along with the other weather variables, consistent with the statewide meteorological approach described in Section 2.3.1. To quantify human-relevant thermal stress, we computed the heat index (HI) defined as the apparent temperature perceived by humans under given conditions of ambient temperature and humidity [32]. The heat index was chosen over dry-bulb temperature as the exposure metric

 doi:10.20944/preprints202604.0453.v1

because it captures the combined physiological effect of heat and humidity on human thermoregulation and on heat-sensitive infrastructure components (e.g., transformers, overhead conductors), which degrade more rapidly under high humidity when convective cooling is impaired [24]. We employed the standard Rothfusz regression used by the U.S. National Weather Service [24,33], which is the most widely used heat-index formulation in U.S. climate and public-health applications. Air temperature was first converted to Fahrenheit ($T_{d,f} = T_d \times 9/5 + 32$), and the heat index (°F) was then computed as:

$$\mathrm{HI} = -42.379 + 2.04901523\,T_F + 10.14333127\,RH - 0.22475541\,T_F RH - 6.83783 \times 10^{-3}\,T_F^2 - 5.481717 \times 10^{-2}\,\mathrm{RH}^2 + 1.22874 \times 10^{-3}\,T_F^2\,\mathrm{RH} + 8.5282 \times 10^{-4}\,T_F RH^2 - 1.99 \times 10^{-6}\,T_F^2\,RH^2$$

Following NWS guidelines, when $T_F < 80$ °F or RH < 40%, the heat index was set equal to the dry-bulb air temperature ($\mathrm{HI} = T_F$) because the polynomial regression was derived from Steadman's model for conditions of $T_F \geq 80$ and RH > 40% and is not calibrated outside this range [32,33]. This conditional application avoids extrapolation artifacts under mild conditions where heat-index adjustments are negligible. The heat index has been shown to outperform dry-bulb temperature as a predictor of both heat-related mortality and electricity demand, making it a suitable exposure metric for studies linking thermal stress to infrastructure outcomes [24].

2.4. Daily Metrices

Hourly records were aggregated to daily county-level metrics for each county *c* and calendar day *d*. Daily aggregation was chosen as the standard temporal resolution as heatwave definitions in both meteorological and public-health literature are inherently day-based and daily metrics effectively capture the cumulative thermal stress placed on the distribution system over each diurnal cycle [2,34]. We computed the following variables:

- **Temperature:** daily maximum ($T_{F,\,max} = \max_{h \in d} T_{F,h}$), and daily mean ($T_{F,mean} = \mathrm{mean}_{h \in d}\, T_{F,h}$) air temperature (°F).
- **Heat index:** daily maximum ($\mathrm{HI}_{max} = \max_{h \in d} \mathrm{HI}_h$), and daily mean ($\mathrm{HI}_{mean} = \mathrm{mean}_{h \in d}\, \mathrm{HI}_h$). The daily maximum heat index serves as the primary heatwave indicator because it captures the peak thermal stress experienced during the hottest part of the day, when electricity demand and equipment thermal limits are most critical [2].
- **Hours of extreme heat:** the number of hours during which the heat index equaled or exceeded 95 °F ($n_{HI \geq 95} n_{HI \geq 95}$) and 100 °F ($n_{HI \geq 100} n_{HI \geq 100}$). These counts characterize the duration of sustained extreme heat within each day, complementing the peak value with a measure of persistence.
- **Outage metrics:** total new outage customers during the day ($\mathrm{new\_outages\_day}_{c,d} = \sum_{h \in d} \mathrm{new\_outages}_{c,h}$) and the maximum concurrent customers without power ($\mathrm{max\_outages\_customers}_{c,d} = \max_{h \in d} \mathrm{outages\_customers}_{c,h}$). The daily sum of new outages captures total failure magnitude, while the daily maximum concurrent outage reflects peak system stress.
- **Month:** extracted from the date for subsequent seasonal filtering.

2.5. Adaptive Heatwave Threshold

Heatwave days were identified using a data-driven percentile-based method that adjusts to the local warm-season climate, following recommended practices in heatwave research [2]. A percentile-based approach was chosen over a fixed absolute threshold (e.g., 105 °F) for two reasons. First, fixed thresholds may be too stringent in some climates and too lenient in others, leading either to too few events for meaningful statistical analysis or to the inclusion of routine warm days that do not represent genuine heatwave stress [2]. Second, percentile-based definitions adapt naturally to the climatological baseline of the study region, ensuring that identified heatwave days represent truly anomalous thermal conditions relative to local norms—a property that is critical when examining

 doi:10.20944/preprints202604.0453.v1

infrastructure impacts, as power systems are typically engineered to tolerate normal summer temperatures but may fail under conditions that exceed historical design margins [35,36].

The daily dataset was first restricted to warm-season months (May through September, i.e., months 5–9). This five-month window was selected because it encompasses the full warm season in Texas, during which virtually all heatwave events occur, and is consistent with the seasonal bounds used in prior U.S. heatwave studies [2,3,21]. We only retained rows with valid (non-missing) daily maximum heat index values and constructed the empirical distribution of HI_{max} across all counties and years. For candidate percentiles $q \in \{0.95, 0.90, 0.85, 0.80\}$, the corresponding heat index threshold $T_{HW}(q)$ was computed and two sufficiency criteria were evaluated. First, the total number of warm-season county-days exceeding the threshold must reach at least 200 (i.e., $N_{HW,} \geq$ MIN_HW_DAYS = 200. Second, the number of those exceedance days that also recorded at least one new outage must reach at least 20 (i.e., $N_{HW,out} \geq$ MIN_OUTAGE_HW_DAYS = 20.

These dual sufficiency criteria serve a specific analytical purpose. Criterion (i) ensures that the heatwave definition identifies a sufficient number of heat-stress days for robust distributional analysis, preventing the threshold from being so extreme that only a handful of days qualify. Criterion (ii) ensures adequate co-occurrence between heatwave conditions and observed outages, which is essential for the subsequent logistic regression to have sufficient positive cases in both the event and non-event classes. Without this overlap condition, an excessively stringent threshold could yield heatwave days with no recorded outages, rendering the heat–outage relationship not estimable.

The first (i.e., most stringent) percentile q^* satisfying both criteria was selected to maximize the climatological extremity of the heatwave definition while maintaining statistical feasibility. If no candidate percentile met these criteria, the analysis defaulted to q = 0.80; if that also failed, a fixed absolute fallback of 90 °F was applied. A county-day was then classified as a heatwave day if it fell within the warm season and its daily maximum heat index equaled or exceeded T_{HW}:

$$is\_heatwave\_day_{c,d} = 1\,[month(d) \in \{5,\ldots,9\} and\ HI_{max,c,d} \geq T_{HW}]$$

This adaptive design ensures that the heatwave definition reflects the regional climate while guaranteeing adequate overlap between identified heatwave days and reported outages for robust statistical analysis. The percentile-based approach is analogous to methods used in heat-mortality studies [24,37] and heat-infrastructure research [16,30].

2.6. Heatwave Event Identification and Metrics

We first classified warm-season days as heatwave or non-heatwave based on the chosen HI threshold and then defined heatwave events as continuous sequences of heatwave days. For each county, we sorted days chronologically and a new event was initiated whenever a heatwave day followed a non-heatwave day, or a gap of more than one calendar day occurred between consecutive heatwave days. Heatwave events were required to last at least two days ($L_e \geq 2$), consistent with standard meteorological and public health practices [2,34]. If this condition produced no events with outages for a county, the threshold was relaxed to $L_e \geq 1$ to prevent exclusion of short but severe heat episodes coincident with outages.

For each heatwave event *e*, hourly records were joined by county FIPS code and date, and the following event-level metrics were computed:

(i) start and end times: $t_{start,e}$ = min(datetime_hour), $t_{end,e}$ = max(datetime_hour)

(ii) Duration (hours): $L_e = \frac{t_{end,e} - t_{start,e}}{3600} + 1$; where the additive term of one hour ensures that single-hour events receive a non-zero duration and that events spanning n consecutive hours are correctly counted. We chose duration in hours (rather than days) to capture sub-daily differences in event persistence, enabling finer-grained comparisons of outage duration across events of nominally similar day-counts.

This event-based representation links an episode's integrated heat conditions to its outage characteristics, supporting both descriptive distributional analyses and regression modeling [19,29].

 doi:10.20944/preprints202604.0453.v1

2.7. County-Level Indicators and Mapping

To visualize spatial patterns, event data were aggregated to county-level indicators. County-level aggregation was chosen because it matches the spatial resolution of both the EAGLE-I outage data and the administrative units used in emergency management and utility service territory planning, enabling results to inform county-level preparedness and resource allocation decisions [38,39]. For all heatwave events (regardless of outage), we computed number of heatwave events and mean duration. For outage-bearing events, we computed: (1) number of heatwaves–outage events, (2) total peak customers affected, and (3) mean event duration.

To prevent a small number of highly affected counties from dominating the color scale, the total peak customers map was capped at the 90th percentile, with values above this cutoff set to that threshold. This approach preserves the spatial distribution of the variable while preventing extreme outliers from dominating the visualization, a common practice in choropleth mapping of skewed infrastructure and hazard data [38]. Choropleth maps used sequential color schemes where darker colors indicate higher frequency, larger impacts, or longer durations, consistent with recommended practice for climate–infrastructure risk mapping [16,21].

2.8. Exploratory Distributions of Event Severity and Duration

Histograms were constructed to characterize the distributions of outage severity and event duration. For events with outages, we produced three panels. First, the full distribution of maximum customers affected (logarithmic y-axis) showing whether the severity distribution is approximately normal, log-normal, or heavy-tailed information that directly informs the modeling strategy adopted in Section 2.9. Second, a detail view restricted to 0–30 customers (linear scale), revealing the high frequency of very small events that dominate the distribution. Lastly the full distribution of event durations (log y-axis) showing how long heatwave–outage events typically persist (Section 2.7). Because both severity and duration are heavy-tailed, counts were plotted on a logarithmic scale. These panels motivate the focus on major events in the regression analysis, consistent with prior work on storm-related outages [19].

2.9. Logistic Regression for Major Outages

2.9.1. Definition of Major Events

Rather than applying simple linear correlations which may be inadequate given heavy-tailed severity distributions and many zero-outage days [20] we focused on the probability of major outage events as a function of heat intensity at the event level. We converted the continuous severity metric (M_e, the maximum number of customers simultaneously affected during heatwave event e, i.e., maximum customers, M_e) into a binary major-event indicator under three alternative thresholds:

- **P90 severity:** $M_e \geq P_{90}$, events in the top 10% of severity (≥347 customers in the dataset);
- **P95 severity:** $M_e \geq P_{95}$, events in the top 5% of severity (≥1,047 customers)**;**
- **Fixed 500 customers:** operationally interpretable utility-scale threshold

Percentile-based cutoffs ensure "major event" corresponds to statistically rare upper-tail outages, while the fixed 500-customer threshold adds an engineering criterion. Testing multiple thresholds demonstrates robustness of the heat–risk relationship across plausible severity definitions, rather than being an artifact of a single threshold choice [16].

2.9.2. Model Specification

For each of the three severity thresholds defined above (P90, Fixed 500, and P95; collectively denoted as τ), we fit a logistic regression with the centered event-mean heat index as predictor ($X_e = HI_{mean,e} - \mu_{mean}$) where μ_{mean} the grand mean of event-mean heat index across all N heatwave events. The logistic model estimates the log-odds of a major event as a linear function of X_e, with parameters estimated by maximum likelihood [40]. The heat intensity effect is summarized as an odds ratio (OR)

 doi:10.20944/preprints202604.0453.v1

per +1 °F increase in event-mean HI, with 95% confidence intervals. We report Wald p-values for the null hypothesis $\beta_1 = 0$ and McFadden's pseudo-R^2 as a goodness-of-fit measure [40].

Logistic regression is preferable to ordinary least squares because the response variable is binary (e.g., occurrence of an outage vs. none). Because the outage severity distribution is highly skewed and zero-inflated, the logistic model is appropriate as it can directly estimate the change in probability of a major outage as heat increases.

2.9.3. Visualization of Fitted Relationships

For each threshold model, we plotted the fitted probability curve and jittered binary observations together. This visualization shows how the probability of major outages increases with event-level heat intensity, enabling direct comparison across severity thresholds. This event-based structure extends recent work on climate and outage risk to the specific context of heatwave-driven failures in Texas [29,41].

2.10. Notation Summary

Table 1 summarizes the principal symbols and subscripts used throughout the Methods and Results sections.

Table 1. Summary of principal symbols and their definitions.

Symbol	Definition	Units
c	County index (one of 254 Texas counties)	—
h	Hour index	—
t	Timestamp within hour h	—
y	Calendar year	—
T	Air temperature	°C
RH	Relative humidity	%
T_d	Dew point temperature (derived via Magnus–Tetens from T and RH)	°C / °F
T_F	Air temperature converted to Fahrenheit	°F
HI	Heat index (apparent temperature as perceived by humans)	°F
HI_{max}	Daily maximum heat index for county c on day d	°F
HI_{mean}	Mean heat index over a heatwave event e	°F
T_{HW} (q)	Adaptive heatwave threshold at candidate percentile q	°F
q*	Selected percentile threshold satisfying sufficiency criteria	—
L_e	Duration of heatwave event e	hours
$outages\_customers_{(c,h)}$	Maximum concurrent customers without power in county c during hour h	customers
$new\_outages_{(c,h)}$	New (incremental) outage customers in county c during hour h	customers
M_e	Maximum customers simultaneously affected during heatwave event e	customers
X_e	Centered event-mean heat index: $X_e = HI_{mean}\_e - \mu$	°F
μ	Grand mean of event-level HI_{mean} across all events	°F
τ	Severity threshold defining a major outage event (P90, P95, or 500 customers)	customers
OR	Odds ratio per +1 °F increase in X_e from logistic regression	—
β_1	Logistic regression coefficient for X_e	—
R^2	McFadden pseudo-R^2 (goodness-of-fit)	—
N_{HW}	Number of warm-season heatwave days exceeding T_{HW}	days

 doi:10.20944/preprints202604.0453.v1

Symbol	Definition	Units
$N_{HW,out}$	Number of heatwave days coinciding with at least one outage	days

2.11. Software and Reproducibility

All analyses were coded in Python 3 using open-source tools: Pandas and NumPy for data processing, GeoPandas for spatial operations, Matplotlib for figures, and statsmodels for logistic regression. A complete Google Colab script that generates all tables (CSV/XLSX) and figures (PNG/JPEG) from the article will be provided upon request, ensuring full reproducibility.

3. Results

3.1. Meteorological Data and Spatial Validation

To validate the single-point meteorological approach, we analyzed temporal correlations of daily maximum heat index across eight representative locations spanning Texas's diverse climate zones (humid subtropical, semi-arid, and arid). During the warm season (May–September), in Figure 2 pairwise correlations ranged from 0.453 to 0.881 (mean = 0.70), demonstrating that thermal conditions evolve synchronously across Texas despite regional climate differences (Table 2).

Heatwave timing agreement across Texas location in Figure 3 indicates strong temporal coherence in heatwave timing across the eight representative Texas locations. Pairwise, agreement in daily heatwave status was consistently high, ranging from 89.5% to 97.3% across all location pairs. The Central location has especially high agreement with most other sites, often around 94% to 97%. Even the lowest pairwise agreement is still 89.5%. As a result. Figure 3 supports the idea that a single-point meteorological representation can capture the timing of major heatwave days reasonably well across Texas, and the same hot days are usually being identified across the state. It does not mean all locations have identical temperatures every day; rather, it shows that the timing of heatwave events is largely shared statewide.

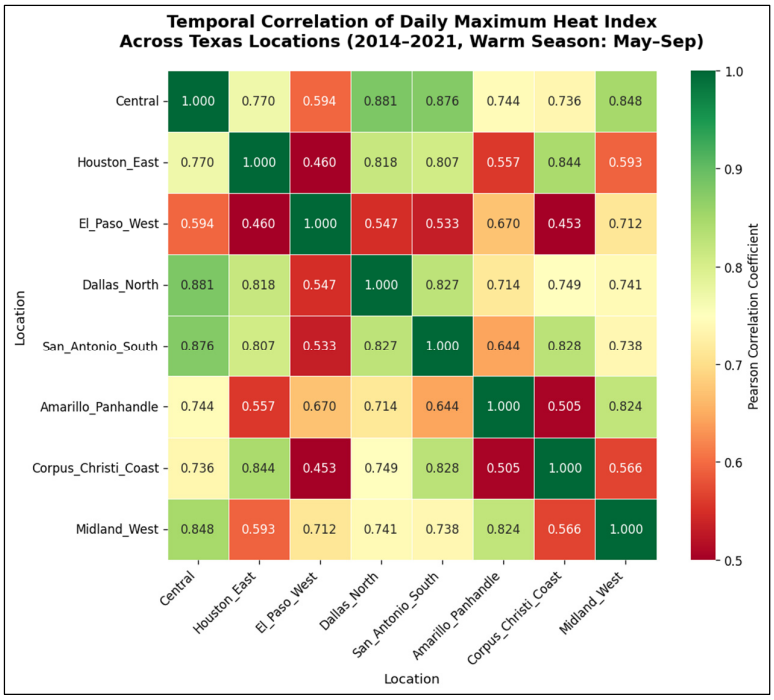

 doi:10.20944/preprints202604.0453.v1

Figure 2. Temporal Correlation of Daily Max HI across Texas selected texas locations (2014-2021) Warm Seasons (May-Sept).

Table 2. *Summary Statistics Spatial Validation.*

Metric	Value	Interpretation
Mean Correlation (all months)	0.9	Temporal correlation of heat index - Strong temporal coherence
Mean Correlation (warm season)	0.70	Temporal correlation (warm season only, may-sep) (Figure 2)
Mean Agreement (%)	92.8	Heatwave timing agreement (Figure 3)
Central vs All (mean corr)	0.922	Correlations with central texas (reference point) - Reference point representative

A summary statistic has been provided in Table 2 for reference. These results confirm that synoptic-scale atmospheric patterns produce spatially coherent heatwave episodes across Texas, where a central reference point is used to identify statewide heatwave periods. While local temperature variations exist, the timing and duration of major heat events are primarily determined by large-scale high-pressure systems affecting the entire region simultaneously.

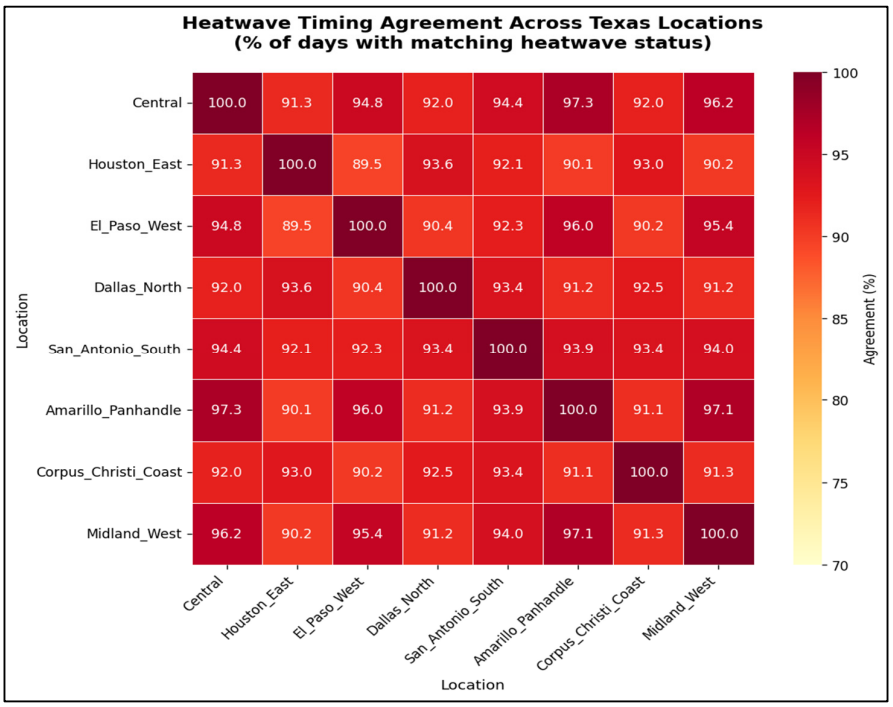

Figure 3. Heatwave Timing Agreement Across Texas Locations.

This approach is consistent with heat-health studies that use representative stations to identify synoptic heat episodes for mortality risk assessment [24]. While future work should employ gridded meteorological datasets to resolve local-scale temperature variations that may influence neighborhood-level outage patterns, the single reference point is appropriate for the event-based framework employed here, where the primary scientific question concerns the temporal relationship between heatwave episodes and observed grid failures at the statewide scale.

The hourly meteorological data was applied uniformly to all 254 Texas counties, consistent with the statewide heatwave-detection approach. This method captures the large-scale thermal forcing

 doi:10.20944/preprints202604.0453.v1

responsible for regional heat stress while acknowledging that it does not resolve intra-state spatial heterogeneity in absolute temperature values.

3.2. Characteristics of Texas Heatwave-Outage Events

Using the adaptive heatwave definition, we identified 3,048 heatwave events across Texas from 2014 to 2021. Of these, 1,551 (approximately 51%) involved at least one customer outage. Outage associated heatwave events were observed in 252 of the 254 counties, demonstrating that heat-related reliability challenges affect virtually the entire state.

Among events with outages, the average maximum number of customers affected was modest at 35. However, the distribution was highly skewed: the 90th, 95th, and 99th percentiles were approximately 1,010, 2,730, and 7,940 customers, respectively. Event durations followed a similar pattern. The median duration was 96 hours (~4 days), with the upper quartile at 120 hours and the 90th percentile at 216 hours (~9 days). These distributions are shown in Figure 4.

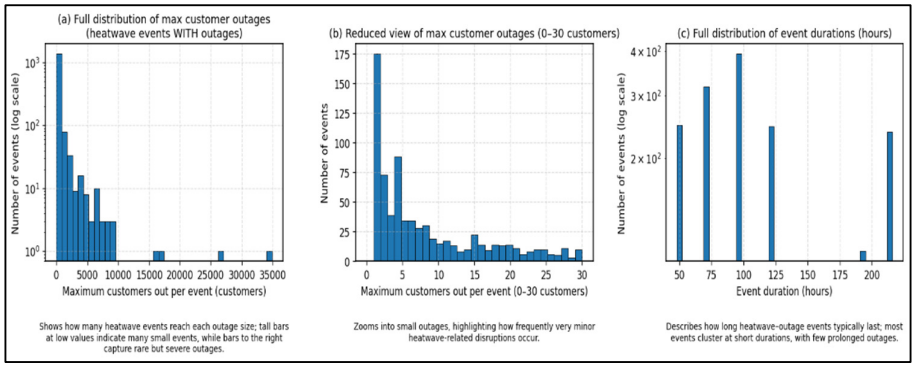

Figure 4. Distributions of event severity and duration for heatwave events with outages: (a) full distribution of maximum customers affected per event (log y-axis); (b) detail view for 0–30 customers (linear scale); (c) full distribution of event durations in hours (log y-axis).

The maximum number of customers affected per event is highly right-skewed (Figure 4a) with most events involving fewer than 100 customers and a small number of extreme events exceeding 10,000 customers. Figure 4b reveals that very small disruptions are highly frequent the modal event size is only a few customers, indicating that Texas heatwaves produce many small, localized disturbances. Figure 4c displays the full distribution of event durations on a log scale, highlighting that most events are short to moderate in length while a minority last a week or longer. Durations cluster at distinct plateaus (approximately 48–216 hours), consistent with the multi-day nature of regional heatwave episodes.

Together, these distributions confirm that heatwave-related outages are dominated by frequent, low-severity events. However, a small number of extreme events account for a disproportionate share of customer impacts and restoration workload. This heavy-tailed structure is consistent with national analyses using the same EAGLE-I platform, which document similarly right-skewed severity distributions across U.S. regions exposed to compound weather stressors [27,38]. The validated EAGLE-I dataset employed here spanning county-level records at 15-minute intervals provides one of the most comprehensive open-source records of distribution-level outages available for the contiguous United States [27], lending additional confidence in the representativeness and reproducibility of the event-based metrics derived in this study.

3.3. Spatial Patterns of Heatwave–Outage Frequency, Impacts, and Duration

County-level summaries reveal clear spatial differentiation in how Texas customers experience heat-related outages (Figures 5–7).

 doi:10.20944/preprints202604.0453.v1

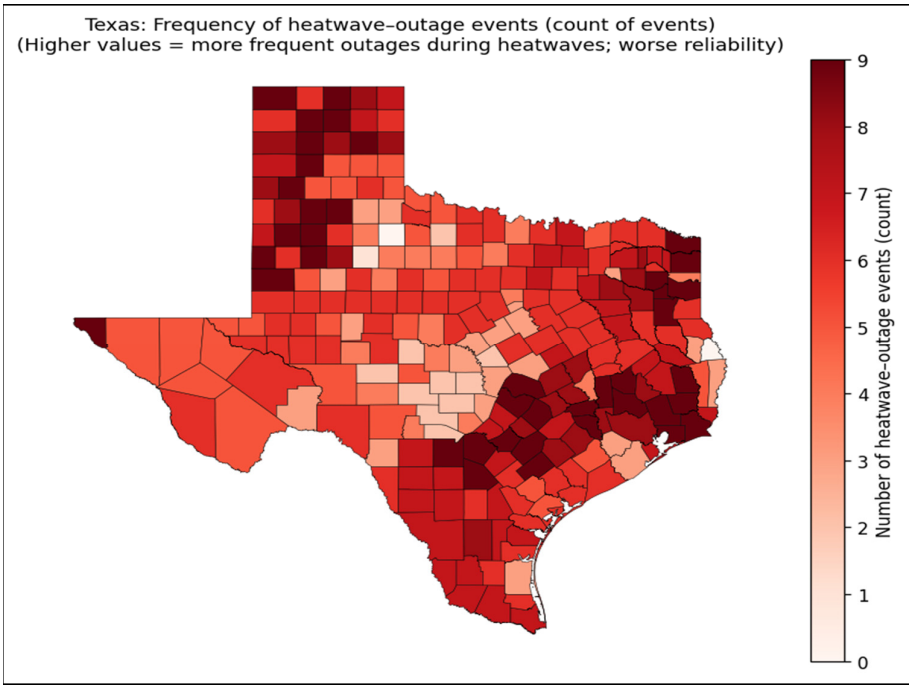

Figure 5. Frequency of heatwave–outage events per county, Texas, 2014–2021.

Figure 5 shows that most counties experienced 3 to 9 heatwave–outage events over the study period. Clusters of higher counts (7–9 events) appear in parts of the Panhandle, north Texas, and the eastern Piney Woods region, suggesting that heatwaves frequently place stress on distribution networks in both rural and urban settings. The Panhandle and Piney Woods counties are largely rural yet show elevated event counts, indicating that rural distribution networks face recurring heat stress. At the same time, high-count counties overlap with major urban corridors such as Dallas–Fort Worth and Houston, where dense load infrastructure heightens outage exposure during extreme heat.

The spatial distribution of total peak customers (Figure 6) demonstrates that high values are concentrated around major load centers including the Houston–Galveston coastal region, the Dallas–Fort Worth metroplex, and parts of south Texas. Due to large customer bases in these regions, even modest increases in outage frequency could translate into significant population exposure. Many rural counties show similar event frequencies but substantially lower exposure, underscoring that event frequency and population impact are distinct dimensions of heatwave–outage risk.

In terms of event duration, most counties experienced around 100–120 hours of power outages for the period of 2014-2021 (Figure 7). However, some areas in west, central, and east Texas exhibit longer average durations (130–170 hours), suggesting that restoration takes longer during heatwave conditions in these areas, possibly due to network topology, access constraints, or resource limitations.

Taken together, the maps demonstrate that heatwave–outage risk in Texas is multidimensional: counties may face more frequent events, larger customer impacts, or longer recovery times, in varying combinations. The event-based indicators allow these dimensions to be visualized and analyzed separately rather than collapsed into a single composite index. The concentration of high customer exposure in major urban corridors demonstrated in this study agrees with the results from a national analysis of 2018–2020 EAGLE-I records, which identified that Southern counties face a dual burden of frequent long-duration outages and elevated social vulnerability, with anomalous heat among the leading co-occurring climate events [42]. Future integration of social vulnerability indices with the event-level indicators presented here could help identify Texas counties where heatwave-related outage exposure intersects most severely with population health needs [43,44].

 doi:10.20944/preprints202604.0453.v1

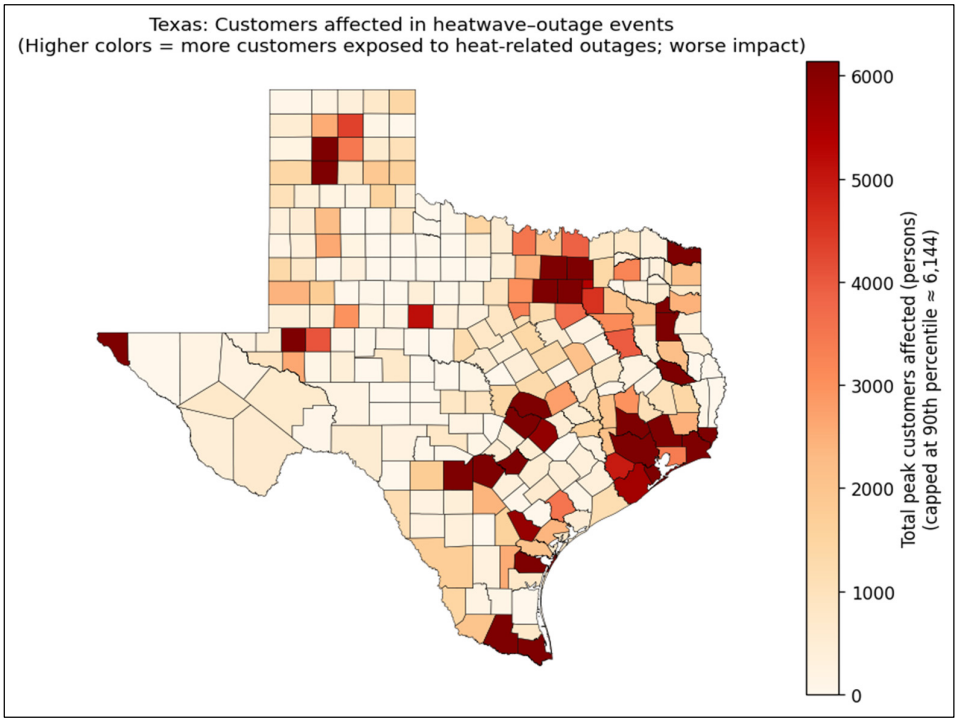

Figure 6. Total peak customers affected across all heatwaves–outage events per county (values capped at the 90th percentile, ~6,100 customers, to preserve color scale legibility).

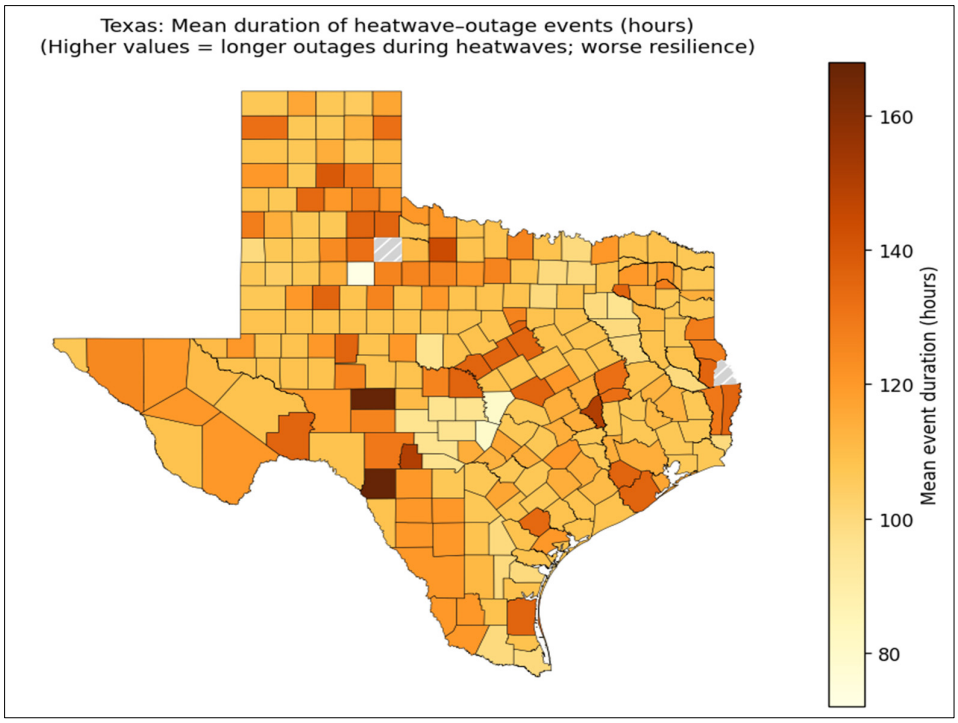

Figure 7. Mean duration (hours) of heatwave–outage events per county, Texas, 2014–2021.

3.4. Major-Outage Logistic Regression and Threshold Robustness

To test the linkage between intense heatwaves and severe outages, we estimated logistic regression models under three severity thresholds: P90 (≥347 customers), P95 (≥1,047 customers) and

 doi:10.20944/preprints202604.0453.v1

Fixed 500 customers. Across all 3,048 heatwave events, the models produced odds ratios ranging from 1.43 to 1.52 per +1 °F increase in mean event heat index. All slopes were highly statistically significant ($p < 10^{-6}$), and McFadden pseudo-R^2 values were between 0.022 and 0.035 (Table 3).

Table 3. Summary of major-outage logistic regression results across three severity thresholds.

Threshold	Key Statistics	Interpretation
P90 (≥347 customers)	OR = 1.52; 95% CI [1.36, 1.70]; p ≈ 4.7×10^{-14}; McFadden R^2 = 0.035	Each +1 °F raises odds of a major event by ~52%. Predicted probability increases from ~7% to ~14% between lower and upper HI quartiles.
Fixed 500 customers	OR = 1.49; 95% CI [1.32, 1.67]; p ≈ 3.4×10^{-11}; McFadden R^2 = 0.030	Utility-relevant threshold. Each +1 °F increases odds of a ≥500-customer event by ~49%. Probability approximately doubles (~5%→~11%) across the observed IQR.
P95 (≥1,047 customers)	OR = 1.43; 95% CI [1.23, 1.65]; p ≈ 1.8×10^{-6}; McFadden R^2 = 0.022	Focuses on the most extreme 5% of events. Absolute probabilities are lower (~3–7%) but the relative increase with heat intensity remains strong.

The logistic probability curves (Figures 8–10) demonstrate the association of the fitted probability of a major outage event and mean event heat index. Jittered binary observations (0/1) and the fitted logistic curve are shown together. For the P90 severe events (Figure 8), the predicted probability of a major outage event approximately doubles from ~7% at the lower quartile of mean heat index (~88.4 °F) to ~14% at the upper quartile (~90.6 °F). For the P95 threshold (Figure 9), the probability rises from ~3% to ~7% across the same interquartile range. For the fixed 500-customer threshold (Figure 10), the corresponding increase is from ~5% to ~11%.

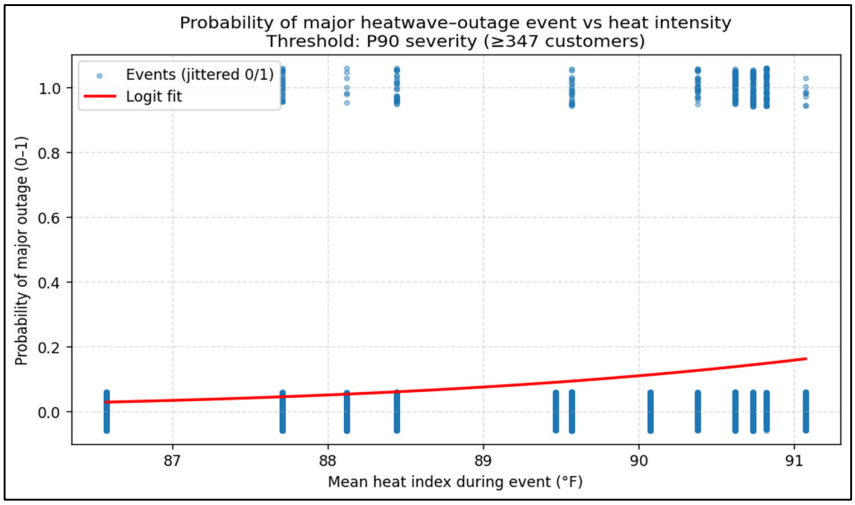

Figure 8. Probability of a major heatwave–outage event versus mean event heat index: P90 severity threshold (≥347 customers). Points represent individual events (jittered); red curve is the fitted logistic model.

 doi:10.20944/preprints202604.0453.v1

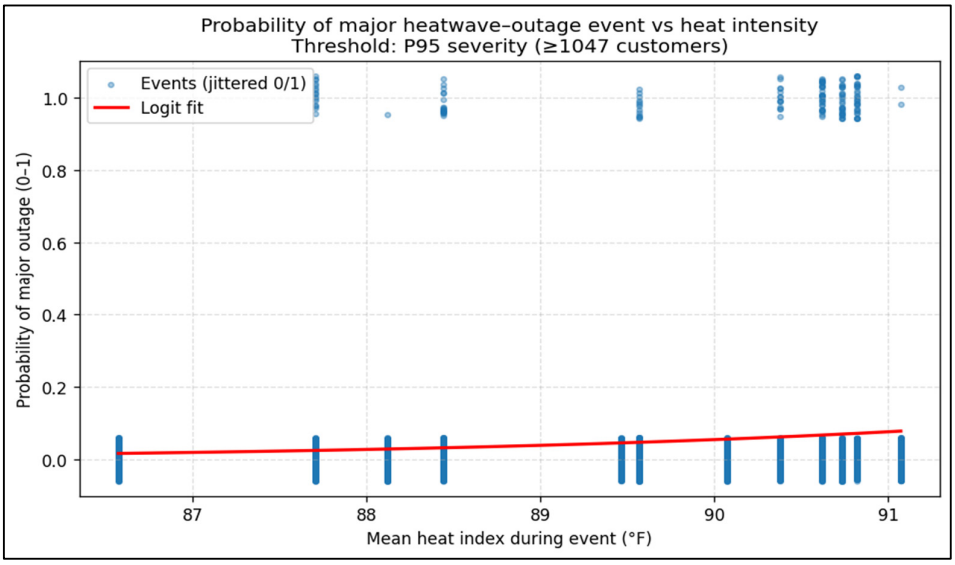

Figure 9. Probability of a major heatwave–outage event versus mean event heat index: P95 severity threshold (≥1,047 customers).

The upward slope in all three panels (Figure 8, 9, and 10) confirms that increased heat intensity raises the probability of crossing any severity threshold, while absolute probabilities remain modest reflecting that heatwaves do not deterministically cause major outages but that warmer heatwaves are consistently more likely to produce them. The odds ratios reported here (1.43–1.52 per +1 °F) are broadly consistent with a parametric outage risk framework applied to the Con Edison distribution grid in New York City, which similarly projected intensifying heatwave-induced outage risk under future climate scenarios due to the compounding of demand increases and infrastructure fragility [30]. That the heat–outage signal persists across all three threshold definitions further supports the robustness of heat index as a probabilistic predictor, echoing national evidence that anomalous heat co-occurs with severe outages across a representative sample of U.S. counties [41].

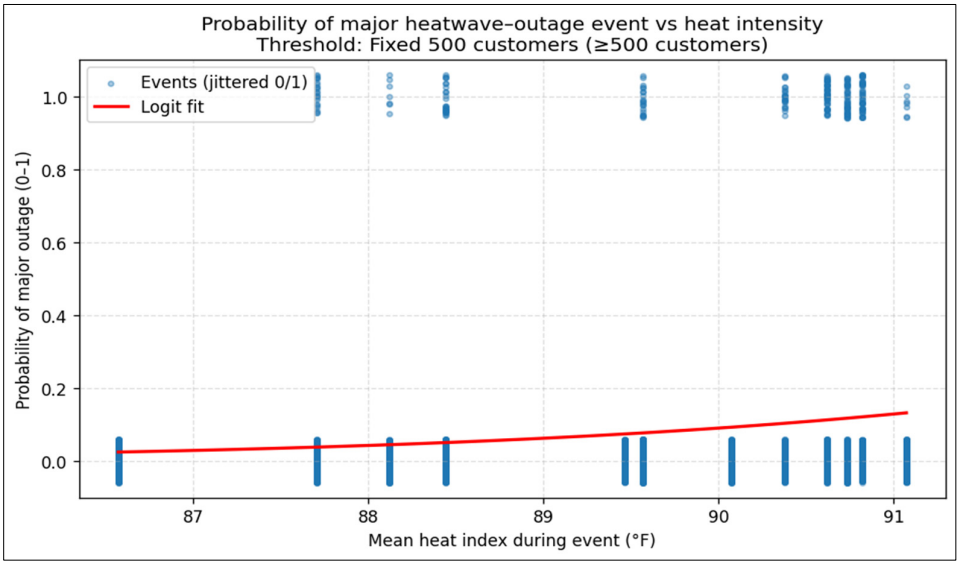

Figure 10. Probability of a major heatwave–outage event versus mean event heat index: Fixed 500-customer threshold.

 doi:10.20944/preprints202604.0453.v1

4. Discussion

4.1. Heat Intensity as a Probabilistic Driver of Major Outages

Our findings demonstrate a strong linkage between heatwave days/events and outage risk. Hotter events last longer and produce higher maximum customer counts. Logistic models indicate that the odds of exceeding major-outage thresholds increase by approximately 43–52% (derived from the logistic regression odds ratios of 1.43–1.52 per +1 °F reported in Table 3, which correspond to a 43–52% increase in the odds of a major outage per degree) for each degree Fahrenheit rise in mean event heat index. This is consistent with global analyses showing that heatwaves amplify outage risks across urban and rural systems due to compounded thermal and demand stresses [1,11].

The low McFadden R^2 values (0.022–0.035) should not be interpreted as evidence that heat is unimportant. Rather, they reflect that outage occurrence is inherently multi-causal, driven jointly by asset condition, vegetation and wind exposure, operational practices, and social factors [35,36]. This conforms to multi-hazard resilience frameworks that recognize heat as one contributor to grid stress among several spatially variable infrastructure vulnerabilities [45–47]. The Texas-specific context adds important nuance: multi-year analysis of EAGLE-I records identifies high heat followed by heavy precipitation as the primary compound driver of the most severe outages in Texas [16], suggesting that the heat-only odds ratios reported here are a conservative lower bound. In years when heatwaves coincide with convective activity or drought-driven vegetation stress, actual outage risk may be substantially higher than heat alone would predict [30], further reinforcing the case for multi-hazard extensions of the current framework.

Our use of the mean heat index rather than air temperature alone captures the combined effect of temperature and humidity on thermal stress and human exposure. The consistent positive relationship between heat index and the probability of exceeding various outage-severity thresholds (Figures 8–10) supports the inference that more intense heatwaves push the power system toward its operational limits, increasing the likelihood of major outages even when other concurrent stressors are present [35,48].

4.2. Comparison with Previous Studies

Most prior research on climate and power system reliability has addressed tropical cyclones, ice storms, or multi-hazard resilience, using wind speed, precipitation, and infrastructure data to predict outages or restoration times [19,20]. In contrast, heatwave-focused research has primarily addressed demand and supply extreme heat increasing cooling loads, reducing thermal plant efficiency, or constraining transmission capacity [29,47] with fewer studies linking heatwave metrics directly to observed distribution-level outages at large scales.

Our study advances this literature in several ways. We apply an adaptive, statistically grounded threshold to the warm season heat index, avoiding reliance on fixed temperature cutoffs or calendar definitions [1,49]. We construct event-level outage metrics amenable to county-level aggregation or probabilistic modeling. By merging EAGLE-I outage records with Open-Meteo archives and heat-index calculations, we develop a reproducible framework applicable to other U.S. states or future climate scenarios.

Rather than adopting a single definition of a "major outage," we compare percentile-based (P90, P95) and fixed-customer thresholds, demonstrating that the heat–outage relationship is robust across all three. This approach bridges statistical modeling and practical planning thresholds, analogous to storm-response studies that separate routine from large-event outages for resource allocation[19]. The open-access orientation of this study is also noteworthy. By relying entirely on the publicly available EAGLE-I archive [27], the Open-Meteo reanalysis API, and reproducible Python tools, this framework lowers the barrier for replication and extension to other states or climate scenarios. A recent national co-occurrence analysis found that 72.7% of contiguous U.S. counties experienced at least one severe weather event co-occurring with an 8-hour or longer power outage over a three-year

 doi:10.20944/preprints202604.0453.v1

period [38], underscoring the broad applicability of event-based outage characterization methodologies like the one developed here.

4.3. Spatial Heterogeneity and Resilience Implications

The county-level maps underscore that heatwave–outage risk is unevenly distributed across Texas. Counties experiencing many events face recurring operational stress during warm seasons, suggesting a need for enhanced vegetation management, targeted hardening, or increased operational flexibility [48,50]. Counties with high peak customer exposure primarily large urban load centers stand to benefit most from demand management, distributed energy resources, and coordinated cooling-center planning during heatwaves. Counties with longer mean outage durations may face constraints related to radial feeder topology, difficult terrain, or limited restoration resources.

By decomposing risk into frequency, exposure, and duration, our analysis provides a multi-dimensional perspective on heatwave resilience that cannot be captured by a single composite index. This granularity supports more targeted and cost-effective intervention planning. The equity dimension of spatial heterogeneity also warrants attention. Research on outage burden in Washington State found that counties with higher poverty and disability rates experience systematically longer outage durations even after controlling weather severity [39]. A parallel analysis of Gulf Coast counties identified heatwaves alongside hurricanes as the events associated with the longest restoration times, with social vulnerability further amplifying recovery disparities [35]. In Texas, major urban load centers face high exposure while rural counties may face constrained restoration capacity explicit integration of social vulnerability data into the event-based indicators developed here would support more equitable grid-hardening and resource-allocation decisions, consistent with emerging equity-centered approaches to infrastructure resilience planning.

4.4. Limitations and Future Work

While the identified relationships are statistically robust, several limitations warrant acknowledgment. First, EAGLE-I data are aggregated by county, preventing feeder-level analysis or community-level vulnerability assessment. The recently published data descriptor for the EAGLE-I archive confirms high coverage rates 92% of U.S. customers by 2022 and provides a formal Data Quality Index by FEMA region [27]; however, the pre-2018 years used in this study had lower utility coverage, which may undercount outages in some counties and should be considered when interpreting early-period trends. Second, heat exposure was estimated using a single central Texas reanalysis grid point, which does not capture sub-state climate heterogeneity. Third, our models omit potential confounders storm activity, vegetation cover, equipment age that may partially explain residual outage variability and co-occur with heat events [23,35].

Future research should employ gridded meteorological datasets (e.g., gridMET, PRISM, or native ERA5 grids) to assign county-specific or census-tract-specific temperature and humidity values. This would enable examination of whether coastal counties with maritime moderation experience different outage responses per degree of heat index compared to interior counties. Additionally, integrating real-time cooling degree days and load data from ERCOT and other Texas utilities would allow direct quantification of the demand-side stress mechanism linking heat exposure to system failure. In future scope of work these gaps can be explored by incorporating spatially distributed meteorological data, region-specific heatwave thresholds calibrated to distinct Texas climate zones, and multi-hazard frameworks that jointly account for heat and storm exposures [24,37]. Feeder-level or utility-level outage data, where available, would enable more granular resilience assessments. Machine learning models integrating infrastructure attributes and demographic exposure could further improve predictive power and support spatially targeted hardening strategies.

Despite these limitations, the consistency of results across multiple thresholds and scales daily versus event level, frequency versus severity versus duration provides strong evidence that heat

 doi:10.20944/preprints202604.0453.v1

intensity is a meaningful and policy-relevant predictor of major outage risk in Texas. As climate change intensifies heatwaves across the southern United States [2,24], our findings suggest that even modest additional warming can substantially raise the odds that a given heatwave produces system-level major outages [47,50], with direct implications for infrastructure planning and public-health preparedness.

5. Conclusions

This study presents a comprehensive, multi-year assessment of how heatwave characteristics influence power outage risk across Texas using an event-based, climatologically adaptive framework. By linking high-resolution outage records with reconstructed heat index data, we demonstrate that heatwaves exert significant and measurable pressure on electric distribution systems at both local and statewide scales.

Although most heatwave-related outages are minor, a small number of extreme events account for a disproportionate share of customer impacts, reflecting the heavy-tailed nature of outage severity. Across all severity thresholds, hotter heatwave events consistently showed a higher likelihood of major outages. Logistic regression results indicate that each incremental increase in mean heat index substantially elevates the odds of severe disruptions, reinforcing heat intensity as an important probabilistic driver of grid failure.

Spatial analyses reveal that outage frequency, population exposure, and restoration duration vary considerably across Texas counties, highlighting the uneven distribution of heatwave vulnerability. These findings underscore the need for targeted grid-hardening strategies, adaptive planning, and resource prioritization in regions most susceptible to extreme heat.

As climate change intensifies the frequency and severity of heatwaves, the methodology developed in this study offers a scalable and reproducible framework for understanding and anticipating heat-driven outage risks. By integrating climate science with infrastructure analytics, this work provides actionable insights that can support utilities, policymakers, and emergency planners in strengthening grid resilience and protecting communities during periods of extreme heat.

Author Contributions: Conceptualization, S.M.R.K. and M.R.; methodology, S.M.R.K.; software, S.M.R.K.; formal analysis, S.M.R.K. and F.K.Z.; investigation, S.M.R.K.; data curation, S.M.R.K.; writing—original draft preparation, S.M.R.K.; writing—review and editing, F.K.Z., M.R., and L.M.; visualization, S.M.R.K.; supervision, M.R. and L.M.; project administration, M.R and L.M. All authors have read and agreed to the published version of the manuscript.

Funding: This research received no external funding.

Data Availability Statement: EAGLE-I outage data are publicly available at https://doi.org/10.13139/ORNLNCCS/1975202. Meteorological data were obtained from the Open-Meteo Historical Weather API (https://open-meteo.com). All analysis results and code is available as a GitHub repository and will be provided upon request.

Conflicts of Interest: The authors declare no conflicts of interest.

References

1. A. C. R. Gonçalves, X. Costoya, R. Nieto, and M. L. R. Liberato, "Extreme weather events on energy systems: a comprehensive review on impacts, mitigation, and adaptation measures," *Sustainable Energy Research 2024 11:1*, vol. 11, no. 1, pp. 4-, Jan. 2024, doi: 10.1186/S40807-023-00097-6.
2. S. E. Perkins, L. V. Alexander, S. E. Perkins, and L. V. Alexander, "On the Measurement of Heat Waves," *J. Clim.*, vol. 26, no. 13, pp. 4500–4517, Jul. 2013, doi: 10.1175/JCLI-D-12-00383.1.
3. R. Wang, C. Yuan, F. Y. Gong, L. Lu, L. Xiang, and X. Wang, "Evaluation and Mitigation of Heatwave-Induced Health Risks in China: A Systematic Review," *Environ. Sci. Technol.*, vol. 59, no. 43, pp. 22987–23004, Nov. 2025, doi: 10.1021/ACS.EST.5C02023.

 doi:10.20944/preprints202604.0453.v1

4. J. Dong, J. Peng, X. He, J. Corcoran, S. Qiu, and X. Wang, "Heatwave-induced human health risk assessment in megacities based on heat stress-social vulnerability-human exposure framework," *Landsc. Urban Plan.*, vol. 203, p. 103907, Nov. 2020, doi: 10.1016/J.LANDURBPLAN.2020.103907.
5. S. Pruckner, J. Bedford, L. Murphy, J. A. Turner, and J. Mills, "Adapting to heatwave-induced seagrass loss: Prioritizing management areas through environmental sensitivity mapping," *Estuar. Coast. Shelf Sci.*, vol. 272, p. 107857, Aug. 2022, doi: 10.1016/J.ECSS.2022.107857.
6. W. Li and R. Sun, "A supply-demand model of vegetation cooling for urban heatwave mitigation," *Urban Clim.*, vol. 52, p. 101699, Nov. 2023, doi: 10.1016/J.UCLIM.2023.101699.
7. Y. ; Zou et al., "Cooling Energy Challenges in Residential Buildings During Heat Waves: Urban Heat Island Impacts in a Hot-Humid City," *Buildings 2024, Vol. 14, Page 4030*, vol. 14, no. 12, p. 4030, Dec. 2024, doi: 10.3390/BUILDINGS14124030.
8. X. Ke, D. Wu, J. Rice, M. Kintner-Meyer, and N. Lu, "Quantifying impacts of heat waves on power grid operation," *Appl. Energy*, vol. 183, pp. 504–512, Dec. 2016, doi: 10.1016/J.APENERGY.2016.08.188.
9. J. Li, J. Wu, Y. Yang, and R. Tang, "Economic consequences of compound drought-heatwave induced power deficits: evidence from Sichuan's 2022 power crisis," *Sustain. Cities Soc.*, vol. 130, p. 106639, Jul. 2025, doi: 10.1016/J.SCS.2025.106639.
10. S. Liu et al., "Underappreciated Emission Spikes From Power Plants During Heatwaves Observed From Space: Case Studies in India and China," *Earths Future*, vol. 12, no. 2, Feb. 2024, doi: 10.1029/2023EF003937.
11. J. Liang, Y. (Lucy) Qiu, B. Wang, X. Shen, and S. Liu, "Impacts of heatwaves on electricity reliability: Evidence from power outage data in China," *iScience*, vol. 28, no. 2, p. 111855, Feb. 2025, doi: 10.1016/J.ISCI.2025.111855.
12. J. Ma, B. Li, O. A. Omitaomu, and A. Mostafavi, "Establishing nationwide power system vulnerability index across US counties using interpretable machine learning," *Appl. Energy*, vol. 397, p. 126360, Nov. 2025, doi: 10.1016/J.APENERGY.2025.126360.
13. L. Rodriguez-Garcia, M. Heleno, and M. Parvania, "Power Distribution System Planning for Mitigating Overheating Risk Inequity," *IEEE Transactions on Power Systems*, vol. 40, no. 1, pp. 920–932, 2025, doi: 10.1109/TPWRS.2024.3418651.
14. B. Stone et al., "How Blackouts during Heat Waves Amplify Mortality and Morbidity Risk," *Environ. Sci. Technol.*, vol. 57, no. 22, pp. 8245–8255, Jun. 2023, doi: 10.1021/ACS.EST.2C09588.
15. B. Zhang, H. Chen, and B. Lu, "An Early Warning System for Heatwave-Induced Health Risks in China: A Sub-Seasonal to Seasonal Perspective — China, 2022," *China CDC Wkly.*, vol. 5, no. 29, p. 647, Jul. 2023, doi: 10.46234/CCDCW2023.124.
16. S. Saki, G. Sofia, B. Kar, and E. Anagnostou, "A multi-year analysis of the impact of heatwaves and compound weather events on power outages," *Scientific Reports 2025 15:1*, vol. 15, no. 1, pp. 30846-, Aug. 2025, doi: 10.1038/s41598-025-15065-x.
17. Y. Li, Y. Tang, S. Wang, R. Toumi, X. Song, and Q. Wang, "Recent increases in tropical cyclone rapid intensification events in global offshore regions," *Nat. Commun.*, vol. 14, no. 1, pp. 5167-, Dec. 2023, doi: 10.1038/S41467-023-40605-2;TECHMETA.
18. C. Yuan, Y. Zhang, Y. Zhou, J. Lin, J. Zhang, and W. Lai, "Analysis of Economic Losses and Comprehensive Impact Factors of Heatwave, Drought, and Heavy Rain Disasters in Hainan Island," *Atmosphere 2025, Vol. 16, Page 1017*, vol. 16, no. 9, p. 1017, Aug. 2025, doi: 10.3390/ATMOS16091017.
19. S. D. Guikema, R. Nateghi, S. M. Quiring, A. Staid, A. C. Reilly, and M. Gao, "Predicting Hurricane Power Outages to Support Storm Response Planning," *IEEE Access*, vol. 2, pp. 1364–1373, 2014, doi: 10.1109/ACCESS.2014.2365716.
20. R. Nateghi, "Multi-Dimensional Infrastructure Resilience Modeling: An Application to Hurricane-Prone Electric Power Distribution Systems," *IEEE Access*, vol. 6, pp. 13478–13489, Jan. 2018, doi: 10.1109/ACCESS.2018.2792680.
21. T. K. R. Matthews, R. L. Wilby, and C. Murphy, "Communicating the deadly consequences of global warming for human heat stress," *Proc. Natl. Acad. Sci. U. S. A.*, vol. 114, no. 15, pp. 3861–3866, Apr. 2017, doi: 10.1073/PNAS.1617526114;SUBPAGE:STRING:FULL.

 doi:10.20944/preprints202604.0453.v1

22. S. Bhattarai, S. Bista, S. Sharma, L. D. White, F. Amini, and R. Talchabhadel, "Spatiotemporal characterization of heatwave exposure across historically vulnerable communities," *Sci. Rep.*, vol. 14, no. 1, Dec. 2024, doi: 10.1038/s41598-024-71704-9.
23. Z. Ma, Z. Zhao, C. Liu, F. Yang, and M. Wang, "The Impacts and Adaptation of Climate Extremes on the Power System: Insights from the Texas Power Outage Caused by Extreme Cold Wave," *https://doi.org/10.1142/S234574812250004X*, vol. 10, no. 1, May 2022, doi: 10.1142/S234574812250004X.
24. B. Anderson and M. L. Bell, "Heat waves in the United States: Mortality risk during heat waves and effect modification by heat wave characteristics in 43 U.S. communities," *Environ. Health Perspect.*, vol. 119, no. 2, pp. 210–218, Feb. 2011, doi: 10.1289/EHP.1002313.
25. V. Tansakul et al., "EAGLE-I Power Outage Data 2014 - 2022," Oak Ridge National Laboratory (ORNL), Oak Ridge, TN. [Online]. Available: https://doi.ccs.ornl.gov/dataset/ccec86f0-e144-5de8-aee0-fb26028b26e1
26. Y.-K. Lim et al., "Remote Forcing and Prediction of the June 2023 Texas Heat Wave," *J. Clim.*, vol. 38, no. 21, pp. 6397–6411, Oct. 2025, doi: 10.1175/JCLI-D-25-0018.1.
27. C. Brelsford et al., "A dataset of recorded electricity outages by United States county 2014–2022," *Scientific Data 2024 11:1*, vol. 11, no. 1, pp. 271-, Mar. 2024, doi: 10.1038/s41597-024-03095-5.
28. H. Hersbach et al., "The ERA5 global reanalysis," *Quarterly Journal of the Royal Meteorological Society*, vol. 146, no. 730, pp. 1999–2049, Jul. 2020, doi: 10.1002/QJ.3803;ISSUE:ISSUE:DOI.
29. M. D. Bartos and M. V. Chester, "Impacts of climate change on electric power supply in the Western United States," *Nature Climate Change 2015 5:8*, vol. 5, no. 8, pp. 748–752, May 2015, doi: 10.1038/nclimate2648.
30. F. Yang, M. Koukoula, S. Emmanouil, D. Cerrai, and E. N. Anagnostou, "Assessing the power grid vulnerability to extreme weather events based on long-term atmospheric reanalysis," *Stochastic Environmental Research and Risk Assessment 2023 37:11*, vol. 37, no. 11, pp. 4291–4306, Jul. 2023, doi: 10.1007/S00477-023-02508-Y.
31. M. G. Lawrence and M. G. Lawrence, "The Relationship between Relative Humidity and the Dewpoint Temperature in Moist Air: A Simple Conversion and Applications," *Bull. Am. Meteorol. Soc.*, vol. 86, no. 2, pp. 225–234, Feb. 2005, doi: 10.1175/BAMS-86-2-225.
32. R. G. Steadman, "The Assessment of Sultriness. Part I: A Temperature-Humidity Index Based on Human Physiology and Clothing Science," *J. Appl. Meteorol. Climatol.*, vol. 18, no. 7, pp. 861–873, Jul. 1979, doi: 10.1175/1520-0450(1979)018.
33. L. P. Rothfusz, "The Heat Index 'Equation' (or, More Than You Ever Wanted to Know About Heat Index)," Fort Worth, TX, 1990. [Online]. Available: https://www.weather.gov/media/ffc/ta_htindx.PDF
34. T. T. Smith, B. F. Zaitchik, and J. M. Gohlke, "Heat waves in the United States: definitions, patterns and trends," *Clim. Change*, vol. 118, no. 3–4, p. 811, Jun. 2013, doi: 10.1007/S10584-012-0659-2.
35. G. Karagiannakis, M. Panteli, and S. Argyroudis, "Fragility Modeling of Power Grid Infrastructure for Addressing Climate Change Risks and Adaptation," *Wiley Interdiscip. Rev. Clim. Change*, vol. 16, no. 1, p. e930, Jan. 2025, doi: 10.1002/WCC.930;REQUESTEDJOURNAL:JOURNAL:17577799;WEBSITE:WEBSITE:WIRES;WGROUP:STRING:PUBLICATION.
36. M. Panteli and P. Mancarella, "Influence of extreme weather and climate change on the resilience of power systems: Impacts and possible mitigation strategies," *Electric Power Systems Research*, vol. 127, pp. 259–270, Oct. 2015, doi: 10.1016/J.EPSR.2015.06.012.
37. A. Gasparrini and B. Armstrong, "The impact of heat waves on mortality," *Epidemiology*, vol. 22, no. 1, pp. 68–73, Jan. 2011, doi: 10.1097/EDE.0B013E3181FDCD99.
38. V. Do, L. B. Wilner, N. M. Flores, H. McBrien, A. J. Northrop, and J. A. Casey, "Spatiotemporal patterns of individual and multiple simultaneous severe weather events co-occurring with power outages in the United States, 2018–2020," *PLOS Climate*, vol. 4, no. 1, p. e0000523, Jan. 2025, doi: 10.1371/JOURNAL.PCLM.0000523.
39. C. A. Richards, S. Amiri, V. P. Walden, J. Postma, M. H. Kapourchali, and A. F. Zuur, "Association of social vulnerability factors with power outage burden in Washington state: 2018–2021," *PLoS One*, vol. 19, no. 9, p. e0307742, Sep. 2024, doi: 10.1371/JOURNAL.PONE.0307742.

 doi:10.20944/preprints202604.0453.v1

40. D. M. Fadden, "Conditional logit analysis of qualitative choice behavior," Frontiers in Econometrics. [Online]. Available: http://elsa.berkeley.edu/reprints/mcfadden/zarembka.pdf
41. V. Do et al., "Spatiotemporal distribution of power outages with climate events and social vulnerability in the USA," *Nature Communications 2023 14:1*, vol. 14, no. 1, pp. 2470-, Apr. 2023, doi: 10.1038/s41467-023-38084-6.
42. G. Karagiannakis, M. Panteli, and S. Argyroudis, "Fragility Modeling of Power Grid Infrastructure for Addressing Climate Change Risks and Adaptation," *Wiley Interdiscip. Rev. Clim. Change*, vol. 16, no. 1, pp. e930–e930, Jan. 2025, doi: 10.1002/WCC.930;REQUESTEDJOURNAL:JOURNAL:17577799;WEBSITE:WEBSITE:WIRES;WGROUP:STRING:PUBLICATION.
43. S. Rao, S. A. Scaggs, A. Asuan, and A. D. Roque, "Power outages and social vulnerability in the U.S. Gulf Coast: multilevel Bayesian models of outage durations amid rising extreme weather," *Humanities and Social Sciences Communications 2025 12:1*, vol. 12, no. 1, pp. 912-, Jun. 2025, doi: 10.1057/s41599-025-05274-0.
44. M. Panteli and P. Mancarella, "Influence of extreme weather and climate change on the resilience of power systems: Impacts and possible mitigation strategies," *Electric Power Systems Research*, vol. 127, pp. 259–270, Oct. 2015, doi: 10.1016/J.EPSR.2015.06.012.
45. S. Aivalioti, "Electricity Sector Adaptation to Heat Waves," *Who's Who*, Jan. 2015, doi: 10.1093/WW/9780199540884.013.U16539.
46. S. Attia et al., "Resilient cooling of buildings to protect against heat waves and power outages: Key concepts and definition," *Energy Build.*, vol. 239, p. 110869, May 2021, doi: 10.1016/J.ENBUILD.2021.110869.
47. G. Hawker, K. Bell, J. Bialek, and C. Maclver, "Management of extreme weather impacts on electricity grids: an international review," *Progress in Energy*, vol. 6, no. 3, p. 32005, May 2024, doi: 10.1088/2516-1083/AD3F6A.
48. A. Dubey, "Preparing the Power Grid for Extreme Weather Events: Resilience Modeling and Optimization," pp. 209–243, 2023, doi: 10.1007/978-3-031-29724-3_8.
49. S. Rao, S. A. Scaggs, A. Asuan, and A. D. Roque, "Power outages and social vulnerability in the U.S. Gulf Coast: multilevel Bayesian models of outage durations amid rising extreme weather," *Humanities and Social Sciences Communications 2025 12:1*, vol. 12, no. 1, pp. 912-, Jun. 2025, doi: 10.1057/s41599-025-05274-0.
50. L. Xu et al., "Resilience of renewable power systems under climate risks," *Nature Reviews Electrical Engineering 2024 1:1*, vol. 1, no. 1, pp. 53–66, Jan. 2024, doi: 10.1038/s44287-023-00003-8.